Small-signal stability analysis of the interactions between voltage source converters and DC current flow controllers

Guan, Rui; Deng, Na; Xue, Ying; Zhang, Xiao-Ping

DOI:
10.1109/OAJPE.2019.2930897

Document Version
Publisher's PDF, also known as Version of record

Citation for published version (Harvard):
Guan, R, Deng, N, Xue, Y & Zhang, X-P 2019, 'Small-signal stability analysis of the interactions between voltage source converters and DC current flow controllers', *IEEE Open Access Journal of Power and Energy*, vol. 7, pp. 2-12. https://doi.org/10.1109/OAJPE.2019.2930897

Received 16 December 2018; revised 4 July 2019; accepted 10 July 2019. Date of publication 5 November 2019; date of current version 2 January 2020.

Digital Object Identifier 10.1109/OAJPE.2019.2930897

Small-Signal Stability Analysis of the Interactions Between Voltage Source Converters and DC Current Flow Controllers

RUI GUAN[1], NA DENG[2], YING XUE[3] (Member, IEEE), AND XIAO-PING ZHANG[3] (Senior Member, IEEE)

[1]Global Energy Interconnection Development and Cooperation Organization (GEIDCO), Beijing 10003, China
[2]Jiangsu Industrial Technology Research Institute (JITRI), Nanjing 210042, China
[3]Department of Electronic, Electrical and Systems Engineering, School of Engineering, University of Birmingham, Birmingham B15 2TT, U.K.

CORRESPONDING AUTHOR: X.-P. ZHANG (x.p.zhang@bham.ac.uk)

This work was supported in part by EPSRC under Grant EP/N032888/1, Grant EP/L017725/1, and Grant EP/K006312/1.

ABSTRACT Small-signal stability analysis of the voltage source converter (VSC) based multi-terminal DC (MTDC) grids has been mainly focused on the dynamics of AC/DC converters while there is a lack of consideration of DC networks with DC power-flow controllers. In this paper, an integrated small-signal model is established to investigate the interactions between VSC and DC current flow controllers (CFC). The impacts of the control system of CFC on small-signal stability of the integrated system and the impacts of the control system of VSC on the DC networks with CFC are discussed via eigenvalue analysis. The above interactions are demonstrated through dynamic simulations against both small and large disturbances using real time digital simulator (RTDS).

INDEX TERMS Small-signal stability analysis, MTDC, VSC high-voltage DC (HVDC) system, CFC.

I. INTRODUCTION

VOLTAGE source converter (VSC) based multi-terminal DC (MTDC) system is the preferred solution for grid connection of large-scale offshore wind farms [1], [2], as it is the feasible option for long distance submarine interconnection of passive and weak systems [3], [4]. For the sake of discussions, Fig. 1 shows a generic topology of MTDC/AC system, which consists of the CFC-integrated DC network and the VSC based AC/DC converter integrated AC network. The AC network includes multiple synchronous generators (G_1 to G_n), multiple VSC converters (VSC_1 to VSC_n), active or passive loads, and/or transmission lines. The DC network consists of DC power-flow controller and DC cables. Previous publications on small-signal stability analysis of VSC MTDC have been focused on the dynamics of VSC (top blue area in Fig. 1) while some other papers have been focused on DC networks with DC power flow controllers (bottom green area in Fig. 1). However, there is a lack of a considerations of these two systems integrated simultaneously using detailed models and hence the potential interactions between them.

With the increasing installations of VSC HVDC systems in power grids, the investigation of controllability and stability

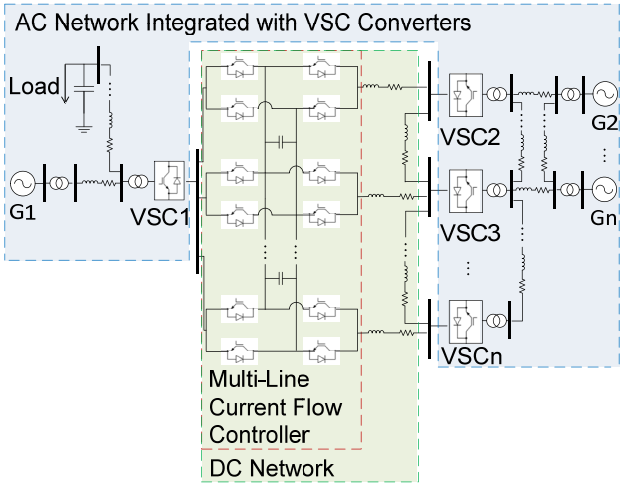

FIGURE 1. Topology of generic MTDC/AC system.

of MTDC systems becomes important for it benefits the existing AC systems with a means of increased energy trading between interconnected system operators [5], [6]. The generalized dynamic model of VSC MTDC was derived

in [7]–[9]. Advanced control extensions with distributed DC voltage control were developed in [10], and a supplementary decentralized control structure to damp interarea oscillations was proposed in [11]. Frequency support function for the surrounding interconnected AC systems and adaptive droop control for effective power sharing through MTDC system were presented and well analyzed in [12], [13]. Electromechanical transient modelling of MMC MTDC was studied in [14] to provide the theoretical foundation for future MMC MTDC applications.

Small-signal stability analysis has been widely used for the study of system dynamics and controller design for VSC [15]–[19]. In [8] the small-signal stability analysis has been carried out for a symmetric bipolar MTDC grid where different modes and interactions between AC systems and VSC following various disturbances were characterized. In [9] small-signal stability analysis was carried out to define the stable operating ranges for the gains of VSC controllers that ensure the dynamic stability of MTDC system. Wind farm generators were considered and a method to calculate converter controller gains was provided. In [12], an adaptive frequency droop control was proposed by investigating the sensitivity of eigenvalues with respect to different droop coefficients, control parameters and changes in operating conditions. In [13], small-signal stability analysis was used for the design of an adaptive droop control scheme. In [20], a method was introduced for systematically identifying interactions of modes in a VSC MTDC system by analyzing the participation pattern from different system elements.

A DC power-flow controller with the use of full-bridge DC-DC converter, which is a relatively small, inexpensive and low-loss device for DC power flow management was proposed in [21], [22]. In [23] a DC power-flow controller was presented to regulate the power flow. In [24], the design of a CFC, along with its control strategy, was proposed which is capable of controlling the DC branch currents to transfer power from an overloaded branch to an underutilized branch to minimize the power loss. Small-signal stability of DC network with CFC was discussed in [25]. A parametric analysis scheme for optimization of control gains of CFC is proposed in [26]. The characteristics, modelling, control, operational performance of different configurations of series-connected CFCs are studied, including dual-thyristor converter CFC, cascaded VSC dc chopper based CFC, and dual H-bridge CFC (2B-CFC) in [27], and resistive based CFC, RC circuit Based CFC, and capacitive based interline CFC in [28]. Distributed CFC, which is based on series interline CFC with extended and simplified topology proposed in [29], is presented in [30] to reduce overload in DC grid with lower CFC voltage, and increase operational area compared to 2B-CFC, when properly located. A coordinated droop control strategy and droop gain evaluation of multi-line CFC is proposed in [31], and coordinated operation control between multiple CFCs is presented in [32]. Small-signal stability of DC network with CFC was discussed in [25], [26], [31].

However, in the work in [25], [26], [31], VSCs are represented as constant current injections and hence the interactions between CFCs and VSCs cannot be studied. The published papers on small-signal stability of VSC MTDC systems have mainly been focused on the dynamics of VSCs while there is a lack of considerations of DC networks with CFC. And there is also a lack of analysis on the potential impacts of DC power-flow controller on existing MTDC system in terms of network stability and dynamic performance under disturbances. Hence there is a real need to fill in the gap of the interactions between DC networks with CFC and AC/DC converters (even more broadly, the detailed representation of connected AC networks).

The aim of this paper is to fill in this gap of the understanding of the interactions between VSC and CFC and the main contributions of this paper are summarized as follows:

1) In the studies, the detailed mathematical models of the integrated AC/DC system consisting of CFC, VSC and AC synchronous machines have been fully implemented.
2) The modal analysis is used to characterize modes, via participation factor matrix, of the integrated AC/DC systems without/with CFC, investigate the impacts of CFC on the integrated AC/DC systems, and design the proposed methodology to derive stable operating range of CFC.
3) The interactions between CFC and VSC are investigated via eigenvalue trajectory studies and dynamic stability analysis.
4) The small-signal stability analysis results are validated in RTDS against small and large disturbances.

II. SMALL-SIGNAL STABILITY MODEL OF THE INTEGRATED AC/DC SYSTEMS WITHOUT/WITH CFC

Fig. 1 shows the generic topology of a generalized AC/DC system, which consists of CFC-integrated DC networks, VSC and AC networks. The CFC integrated AC/DC system model is represented in differential-algebraic equations (DAEs) and is linearized around an equilibrium point in state-space form as:

$$\Delta\dot{x} = \boldsymbol{A}\Delta x + \boldsymbol{B}\Delta u \tag{1}$$

where Δx and Δu are the incremental change of the state variable vector and input vector, $\boldsymbol{A}$ and $\boldsymbol{B}$ are state matrix and input matrix. The left and right eigenvectors of matrix $\boldsymbol{A}$ form participation factor matrix which provides insight into the relationship between states and modes.

A. CFC AND INTEGRATED DC NETWORK MODEL

The CFC model proposed in [25] is used as an example of DC power-flow controller to investigate its impacts on the existing AC/DC system. For example, the topology of a meshed three-terminal DC network with CFC is shown in Fig. 2.

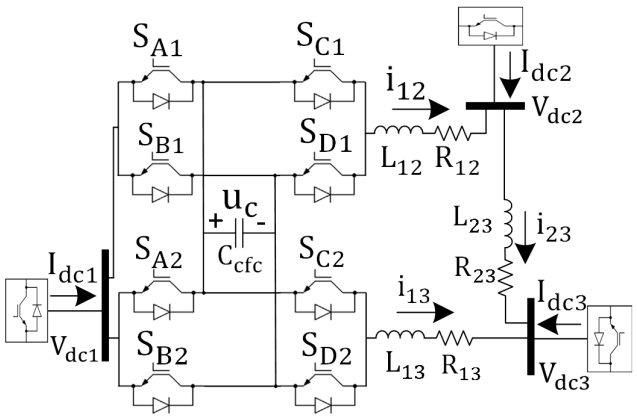

FIGURE 2. DC network with DC CFC.

1) CFC MODEL [25]

The CFC model in [25] is composed of two identical full-bridge DC-DC converters sharing a common capacitor as shown in Fig. 2.

By considering the charging and discharging state of the capacitor within a switching cycle and applying Kirchhoff's voltage law to the DC network, the dynamic equations of three-terminal DC network with CFC can be derived as:

$$C_{cfc}\frac{du_c}{dt} = (d_a - d_{c1})\, i_{12} + (d_a - d_{c2})\, i_{13} \quad (2a)$$

$$L_{12}\frac{di_{12}}{dt} + R_{12}i_{12} = V_{dc1} - V_{dc2} - (d_a - d_{c1})\, u_c \quad (2b)$$

$$L_{13}\frac{di_{13}}{dt} + R_{13}i_{13} = V_{dc1} - V_{dc3} - (d_a - d_{c2})\, u_c \quad (2c)$$

$$L_{23}\frac{di_{23}}{dt} + R_{23}i_{23} = V_{dc2} - V_{dc3} \quad (2d)$$

where u_c is the voltage across capacitor; i_{12}, i_{13} and i_{23} are the DC branch currents for branch 12, 13 and 23; V_{dc1}, V_{dc2}, and V_{dc3} are the DC terminal voltage of VSC_1, VSC_2, and VSC_3; C_{cfc} is the capacitance of the capacitor; R_{12}, R_{13}, and R_{23} represent the resistance of DC branch 12, 13, and 23; L_{12}, L_{13}, and L_{23} represent the reactance of DC branch 12, 13, and 23; d_a represents the switch-on duty cycles of switch S_{A1} and S_{A2}, d_{c1}, and d_{c2} represent the switch-on duty cycles of switch S_{C1} and S_{C2}.

2) CFC CONTROL SYSTEM MODEL

The control system presented in [25], which is to generate gate signals G_{SC1}, and G_{SC2}, is shown in Fig. 3.

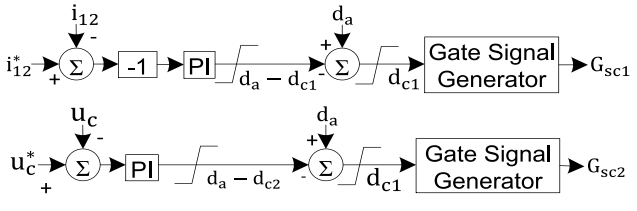

FIGURE 3. Control system of CFC.

In this paper, based on the CFC control system in Fig. 3, the duty cycles d_{c1}, and d_{c2} are calculated as:

$$\begin{aligned} d_{c1} &= d_a - k_{pc1}\left(-i_{12}^* + i_{12}\right) - k_{ic1}\int\left(-i_{12}^* + i_{12}\right)dt \\ &= d_a - k_{pc1}\left(-i_{12}^* + i_{12}\right) - k_{ic1}y_1 \end{aligned} \quad (3a)$$

$$\begin{aligned} d_{c2} &= d_a - k_{pc2}\left(u_c^* - u_c\right) - k_{ic2}\int\left(u_c^* - u_c\right)dt \\ &= d_a - k_{pc2}\left(u_c^* - u_c\right) - k_{ic2}y_2 \end{aligned} \quad (3b)$$

where i_{12}^* is the reference of current through DC branch 12; u_c^* is the reference of voltage across the capacitor; k_{pc1}, k_{ic1}, k_{pc2}, and k_{ic2} are the proportional and integral gains of the CFC PI control loop; y_1 and y_2 are the auxiliary state variables to represent the integral terms of the PI control loop.

The final dynamic equations can be derived by substituting (3) into (2).

B. SYNCHRONOUS GENERATOR MODEL

Each synchronous generator is modeled with a sixth-order model consisting of six state variables as follows:

$$\Delta x = \left[\Delta\delta, \Delta\omega, \Delta E_q, \Delta E_d, \Delta\varphi_{1d}, \Delta\varphi_{2q}\right]^T \quad (4)$$

Then the differential and algebraic equations for synchronous generator i are represented as:

$$\begin{aligned} \Delta\dot{x}_i = \boldsymbol{A_{1i}}\Delta x_i + \boldsymbol{B_{1i}}\Delta\begin{bmatrix}\Delta I_{di}\\ \Delta I_{qi}\end{bmatrix} + \boldsymbol{B_{2i}}\Delta\begin{bmatrix}\Delta\theta_i\\ \Delta V_i\end{bmatrix} \\ + \boldsymbol{E_{1i}}\Delta\begin{bmatrix}\Delta T_{Mi}\\ \Delta V_{refi}\end{bmatrix} \end{aligned} \quad (5)$$

$$\boldsymbol{C_{1i}}\Delta x_i + \boldsymbol{D_{1i}}\Delta\begin{bmatrix}\Delta I_{di}\\ \Delta I_{qi}\end{bmatrix} + \boldsymbol{D_{2i}}\Delta\begin{bmatrix}\Delta\theta_i\\ \Delta V_i\end{bmatrix} = 0 \quad (6)$$

where all the state variables, state matrices, input vectors and input matrices can be found in [18].

First-order IEEE type 2 exciter and third-order power system stabilizer controllers are used with synchronous generators.

C. VSC MODEL

Fig. 4 shows the single-line diagram of a VSC with its control system. dq decoupling control is used. DC voltage or active power is controlled in d-axis, whilst AC voltage at point of common coupling is regulated in q-axis. The dynamic equations of the converter in dq reference frame can be expressed as:

$$v_{cd} - v_{td} = -R_c i_{td} - L_c\frac{di_{td}}{dt} + L_c\omega i_{tq} \quad (7a)$$

$$v_{cq} - v_{tq} = -R_c i_{tq} - L_c\frac{di_{tq}}{dt} - L_c\omega i_{td} \quad (7b)$$

The dynamic equation for DC side capacitor can be expressed as:

$$V_{dc1}\left(I_{dc1} + C\frac{dV_{dc1}}{dt}\right) = \frac{3}{2}\left(v_{cd}i_{td} + v_{cq}i_{tq}\right) \quad (8)$$

where R_c and L_c represents total impedance of the phase reactor and converter transformer.

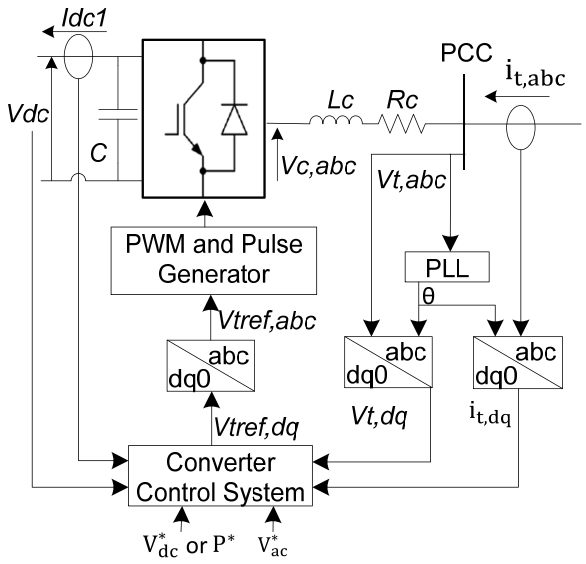

FIGURE 4. **Single-phase diagram of VSC.**

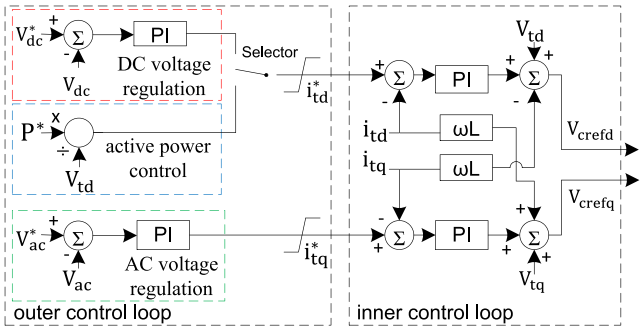

FIGURE 5. **Control loop of VSC.**

1) OUTER CONTROL LOOP: V_{dc} - V_{ac} CONTROL

As the architecture of V_{dc} - V_{ac} control shown in Fig. 5, the current references in dq frame can be obtained from the outer control loop by:

$$\begin{aligned} i^*_{td} &= k_{pdc}\left(V^*_{dc1} - V_{dc1}\right) + k_{idc}\int\left(V^*_{dc1} - V_{dc1}\right)dt \\ &= k_{pdc}\left(V^*_{dc1} - V_{dc1}\right) + k_{idc}x_1 \qquad (9a) \\ i^*_{tq} &= k_{pac}\left(V^*_{ac1} - V_{ac1}\right) + k_{iac}\int\left(V^*_{ac1} - V_{ac1}\right)dt \\ &= k_{pdc}\left(V^*_{ac1} - V_{ac1}\right) + k_{iac}x_2 \qquad (9b) \end{aligned}$$

where k_{pdc}, k_{idc}, k_{pac}, and k_{iac} are the proportional and integral gains of DC voltage and AC voltage controllers. The auxiliary state variables of x_1 and x_2 are used to represent the integral terms of PI controllers.

The AC voltage at point of common coupling V_{ac1} can be represented as:

$$V_{ac1} = \sqrt{v^2_{td} + v^2_{tq}} \qquad (10)$$

2) OUTER CONTROL LOOP: P - V_{AC} CONTROL

As the architecture of P-V_{ac} control mode also shown in Fig. 5, the current reference in dq frame can be obtained as:

$$\begin{aligned} i^*_{td} &= \frac{P^*}{v_{td}} \qquad (11a) \\ i^*_{tq} &= k_{pac}\left(V^*_{ac1} - V_{ac1}\right) + k_{iac}\int\left(V^*_{ac1} - V_{ac1}\right)dt \\ &= k_{pdc}\left(V^*_{ac1} - V_{ac1}\right) + k_{iac}x_2 \qquad (11b) \end{aligned}$$

where k_{pdc}, k_{idc}, k_{pac}, and k_{iac} are the proportional and integral gains of DC voltage and AC voltage controllers. The auxiliary state variable x_2 represents the integral terms of PI control loop.

3) INNER CONTROL LOOP OF VSC

As the converter inner control loop shown in Fig. 5, the reference of VSC converter voltage can be obtained as:

$$\begin{aligned} v^*_{cd} &= k_{pid}\left(i^*_{td} - i_{td}\right) + k_{iid}\int\left(i^*_{td} - i_{td}\right)dt - \omega L_C i_{tq} + v_{td} \\ &= k_{pid}\left(i^*_{td} - i_{td}\right) + k_{iid}x_3 - \omega L_C i_{tq} + v_{td} \qquad (12a) \\ v^*_{cq} &= k_{piq}\left(i^*_{tq} - i_{tq}\right) + k_{iiq}\int\left(i^*_{tq} - i_{tq}\right)dt + \omega L_C i_{td} + v_{tq} \\ &= k_{piq}\left(i^*_{tq} - i_{tq}\right) + k_{iiq}x_4 + \omega L_C i_{td} + v_{tq} \qquad (12b) \end{aligned}$$

where i_{td} and i_{tq} are current components through phase reactor in dq frame; k_{pid}, k_{iid}, k_{piq}, and k_{iiq} are the proportional and integral gains of the current controller; x_3 and x_4 are auxiliary state variables to represent the integral terms of PI control loop.

D. AC NETWORK

The buses of multi-bus AC network can be classified as generator-connected buses and non-generator buses. The power balance equation of a generator connected bus i is:

$$\begin{aligned} V_i e^{j\theta_i}\left(I_{di} - jI_{qi}\right)e^{-j\left(\theta_i - \frac{1}{2}\pi\right)} + P_{Li} + jQ_{Li} \\ = V_i e^{j\theta_i}\sum_{k=1}^{n} V_k e^{-j\theta_k}\left(G_{ik} - jB_{ik}\right) \qquad (13) \end{aligned}$$

where n is the total bus number, P_{Li} and Q_{Li} are the active power and reactive power injection, respectively, to bus i.

Similarly, the power balance equation of a non-generator bus i can be obtained as:

$$P_{Li} + jQ_{Li} = V_i e^{j\theta_i}\sum_{k=1}^{n} V_k e^{-j\theta_k}\left(G_{ik} - jB_{ik}\right) \qquad (14)$$

The values of G_{ik} and B_{ik} can be determined by system network admittance matrix $\boldsymbol{Y}$.

E. FORMULATION OF THE OVERALL LINEARIZED SYSTEM

The complete state-space representation of the multi-model test system is formulated by combining the linearized subsystem models of synchronous generators, VSC, DC network

with CFC, and AC networks. The synchronous generator models are linked with multi-bus AC network model through power flow equations. The VSC models and DC network with CFC model are linked by DC current/voltage relationships. The VSC models are linked to AC network model via power flow equations.

$$\Delta\dot{x} = \boldsymbol{A}\Delta x + \boldsymbol{B}\Delta u \tag{15}$$

where $\boldsymbol{A} = \left[\begin{array}{c|c} \boldsymbol{A_{ACSys}} & 0 \\ \hline 0 & \boldsymbol{A_{MTDC}} \end{array}\right]$, $\boldsymbol{\Delta x} = \left[\boldsymbol{\Delta x_{ACSys}}, \boldsymbol{\Delta x_{MTDC}}\right]^{\boldsymbol{T}}$, $\boldsymbol{B}$ is the input matrix, and Δu is the input vector with references of operating point, submatrix $\boldsymbol{A_{ACSys}}$ and $\boldsymbol{A_{MTDC}}$ represent state matrix of AC systems and MTDC system, $\boldsymbol{\Delta x_{ACSys}}$ and $\boldsymbol{\Delta x_{MTDC}}$ represent state variables of AC systems and MTDC system.

III. INTERACTIONS BETWEEN CFC AND VSC

In Section III, the test system is introduced. Then dynamic analysis of the integrated AC/DC system without and with CFC is studied to investigate the impacts of the incorporation of CFC. Finally, the interactions between CFC and VSC are investigated.

A. TEST SYSTEM

Fig. 6 shows the test system topology of the CFC integrated AC/DC system, which was modified based on the Kundur's 4-generator 2-area system proposed in [15] where parameters can be found. The test system consists of two areas connected by a weak tie (220km transmission line) and a three-terminal AC/DC network. The pole-to-pole DC voltage is 120 kV. A CFC is integrated into the DC network to control DC currents. VSC_2 is operating in V_{dc} - V_{ac} control, controlling the DC voltage and the AC voltage. VSC_1 and VSC_3 are operating in P-V_{ac} control, controlling the active power through converters and the AC voltages. A two-line CFC is installed at the DC side of VSC1 to control current flow from VSC_1 to VSC_3 and VSC_1 to VSC_2. The parameters of the DC network and CFC are shown in Table 1. The control parameters for control system of CFC are from [25] and the control parameters for control system of VSC is based on the approach proposed in [9].

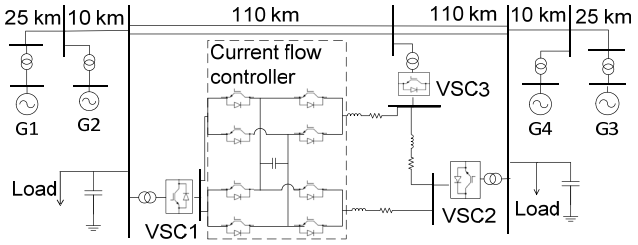

FIGURE 6. Topology of the test system.

B. DYNAMIC ANALYSIS OF THE INTEGRATED SYSTEM WITHOUT/WITH CFC

In order to study the impacts of the incorporation of CFC on small-signal stability of the integrated AC/DC system, eigenvalue analysis is carried out for the system without CFC and the system with CFC. The small-signal stability of the AC/DC system shown in Fig. 6 is to be assessed by modal analysis. The complete state-space matrix of the integrated system without CFC has a dimension of 52 × 52 and complete state-space matrix $\boldsymbol{A}$ of CFC integrated system has a dimension of 55 × 55.The calculated eigenvalues of system with CFC are given in Table 2.

TABLE 1. Parameters of MTDC system.

Parameters	C_{cfc}	C_{VSC}	$R_{12}+L_{12}$	$R_{13}+L_{13}$	$R_{23}+L_{23}$
Values	1 mF	5 mF	1 Ω + 0.07 H	2Ω + 0.09 H	1 Ω+ 0.1 H

TABLE 2. Eigenvalue results.

No.	*Eigenvalue	* Frequency (Hz)	*Damping Ratio	*Dominant State
1	-989.996909	\	\	ΔE_{fd4}
2	-992.295149	\	\	ΔE_{fd1}
3	-995.595105	\	\	ΔE_{fd1}
4	-995.707401	\	\	ΔE_{fd4}
5,6	-29.207818 ± j79.733757	12.690	0.344	Δi_{13}
7,8	-36.172771 ± j74.960903	11.930	0.435	Δi_{12}
9	-50.413402	\	\	ΔV_{pss23}
10	-50.366193	\	\	ΔV_{pss21}
11,12	-21.427289 ± j15.161162	2.413	0.816	$\Delta\varphi_{1d4}$
13	-40.284553	\	\	ΔV_{dc3}
14,15	-36.147588 ± j0.024697	0.004	1.000	$\Delta\varphi_{2q4}$
16	-32.194893	\	\	$\Delta\varphi_{1d2}$
17	-31.405286	\	\	$\Delta\varphi_{1d4}$
18,19	-30.737465 ± j0.158230	0.025	1.000	$\Delta\varphi_{2q2}$
20,21	-20.867725 ± j9.466367	1.507	0.911	ΔE_{q1}
22,23	-1.324673 ± j7.721606	1.229	0.169	$\Delta\delta_2 \setminus \Delta\omega_2$
24,25	-1.353150 ± j7.949151	1.26	0.168	$\Delta\delta_3 \setminus \Delta\omega_3$
26	-13.782411	\	\	Δi_{23}
27	-10.373649	\	\	ΔE_{q1}
28	-10.232547	\	\	ΔE_{q4}
29,30	-0.218588 ± j4.107533	0.654	0.053	$\Delta\delta_1 \setminus \Delta\omega_1$
31,32	-0.554283 ± j0.930014	0.148	0.512	ΔV_2
33	-3.018345	\	\	ΔE_{q3}
34	-3.006447	\	\	ΔE_{d1}
35,36	-3.462913 ± j0.020338	0.003	1.000	ΔE_{d2}
37	-0.204027	\	\	ΔV_{pss31}
38	-0.180561	\	\	ΔV_{pss33}
39,40	-0.092289 ± j0.087653	0.014	0.725	Δx_{32}
41	-0.133912	\	\	Δx_{31}
42	-0.102123	\	\	ΔV_{pss13}
43	-0.051550	\	\	ΔV_{pss11}
44	-0.034554	\	\	Δx_{42}
45	-0.016087	\	\	ΔV_{dc1}
46	-0.011626	\	\	Δx_{31}
47	-0.003970	\	\	Δx_{43}
48	0.000000 + j0.000000	0.000	-0.000	$\Delta\delta_4 \setminus \Delta\omega_4$
49	0.000000 - j0.000000	0.000	-0.000	$\Delta\delta_4 \setminus \Delta\omega_4$
50	-3.333333	\	\	Δx_{21}
51	-3.333333	\	\	Δx_{13}
52	-3.333333	\	\	Δx_{22}
53	-3.333333	\	\	Δx_{12}
54	-3.333333	\	\	Δx_{11}
55	-3.333333	\	\	Δx_{23}

CFC related

CFC related

VSC related

There are 52 eigenvalues for the system without CFC, and 55 eigenvalues for the system with CFC. The additional three states are resulting from the CFC capacitor and 2 integral controllers of CFC (Δu_c, Δy_1, Δy_2). From Table 2, it can be seen that all 55 eigenvalues have non-positive real part. This indicates a stable operating condition around the operating point. There are two zero eigenvalues $\lambda_{48,49}$, as there is no infinite bus bar in the testing system. One zero eigenvalue arises from a redundancy in synchronous generator angle. The second zero eigenvalue results from that the generator torque is independent of machine speed deviations, and this

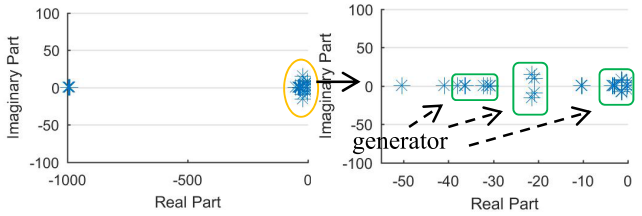

(a) Clustering of eigenvalues (b) Highlighted eigenvalues

FIGURE 7. Eigenvalues of the integrated AC/DC system without CFC.

is caused by the fact that mechanical damping is neglected and governor action is not represented [17].

The eigenvalues $\lambda_{11,12}$, $\lambda_{14,15}$, $\lambda_{18,19}$ to $\lambda_{24,25}$, $\lambda_{29,30}$, and $\lambda_{35,36}$ are related to the dominant state variables of synchronous generators according to their participation factors. The damping of these modes is mainly affected by synchronous generator settings, associated exciter settings, and corresponding PSS parameters. The incorporation of CFC has no significant impacts on these synchronous generator related eigenvalues. The participation matrix also indicates that controller of VSC_3 has dominant influence on $\lambda_{39,40}$. Based on participation matrix, it should be noted that state variables i_{12} and i_{13} of the DC network have dominant influence on the oscillation modes of $\lambda_{5,6}$ and $\lambda_{7,8}$, while auxiliary state variable y_1 of CFC controller dominantly influences $\lambda_{31,32}$. The results of modal analysis show that the incorporation of CFC and its controller parameters affect the small-signal stability of multi-machine AC/DC system.

Fig. 7 shows a plot of eigenvalues of the system without CFC while Fig. 8 shows a plot of eigenvalues of the system with CFC. The dominant states and the associated pairs of eigenvalues are highlighted in Fig. 7 (b) for the system without CFC and in Fig. 8 (b) for the system with CFC. Compared to the system without CFC as shown in Fig. 7 (b), it can be seen that the system with CFC (as shown in Fig. 8 (b)) has 3 additional conjugate pairs of eigenvalues, which are dominated by state variables of DC branch currents i_{12}, i_{13}, and CFC integral controller auxiliary state y_2. Also, the system with CFC has very slight impacts on the generator-related eigenvalues as there are no significant changes in the placements of those eigenvalues. However, the system with CFC leads to the changing of VSC controller related eigenvalues from the pure negative real values to the conjugate pair of

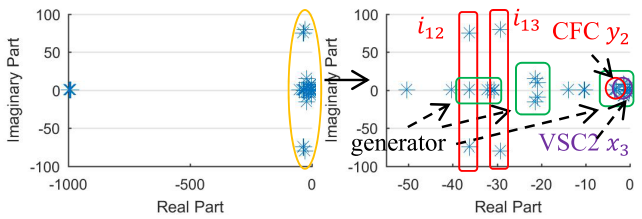

(a) Clustering of eigenvalues (b) Highlighted eigenvalues

FIGURE 8. Eigenvalues of the integrated AC/DC system with CFC.

eigenvalues with negative real part, as highlighted by VSC_2x_3 in Fig. 8 (b). This change results in VSC controller related system oscillations for the system with CFC. This is due to the potential interactions between CFC and adjacent VSC.

From Fig. 8, the critical modes which have major impacts on small signal performance of the system are associated with DC CFC auxiliary state y_2, VSC_2 auxiliary state x_3, and the angle and rotating speed of Synchronous Generator 1.

The AC/DC test system as shown in Fig. 6 has been established in RSCAD to validate the results of modal analysis. The power flow data, AC voltages, and impedance values are based on the 4-generator 2-area benchmark system model in [15], while the parameters of the DC network and CFC are shown in Table 1. The max power loss of CFC, considering conduction and switching loss, is 1.6 MW (1.6% of the system power rating), which is much lower than losses due to the resistances in the DC lines.

1) SIMULATIONS UNDER SMALL DISTURBANCES

Fig. 9 shows the dynamic behavior of the system (controlled DC branch current i_{12}, and voltage across CFC bridge capacitor u_c) in response to a step reference change applied to CFC (i_{12ref} changes from 0.55 kA to 0.50 kA at 0.1s). It can be seen from Fig. 9 that the controlled current of DC branch 12 decreases from 0.55 kA to 0.50 kA. The voltage of DC capacitor returns to its reference value after the small disturbance. Stable dynamic performance can be seen from the simulation results, which is in line with the modal analysis results.

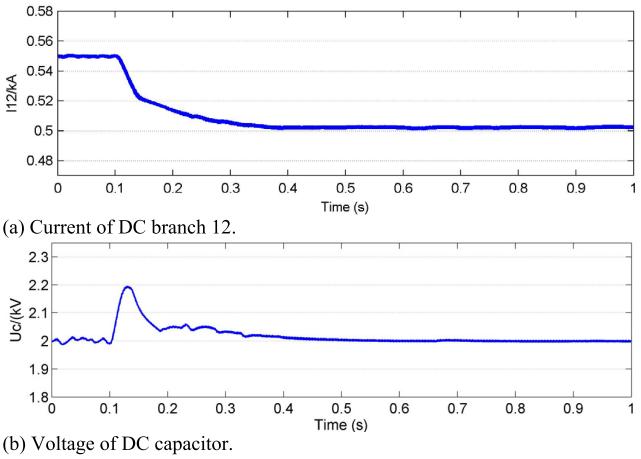

(a) Current of DC branch 12.

(b) Voltage of DC capacitor.

FIGURE 9. Dynamics of DC network during small disturbance.

2) SIMULATIONS UNDER LARGE DISTURBANCES (AC-SYSTEM FAULT)

In this subsection, a large disturbance is applied to test the system stability under large disturbances. A 10Ω single line to ground fault is simulated at the point of common coupling of VSC_3 (primary side of coupling transformer) at 0.3s lasting for 7 cycles (116 ms).

Fig. 10 shows system dynamics of MTDC system, including active power transfer of VSC_1 and VSC_3 (these two converters are in P - V_{ac} control), and current of DC branch 12. The system recovers to steady-state in a short period of time after the fault is cleared. It demonstrates that the system can endure large AC disturbance and recover quickly.

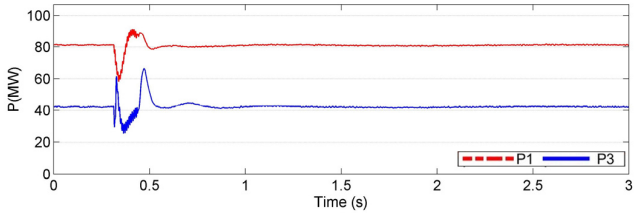

(a) Active power of converters.

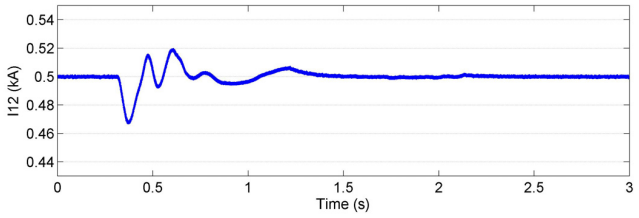

(b) Current of DC branch 12.

FIGURE 10. Dynamics of MTDC system against AC system fault.

3) SIMULATIONS UNDER LARGE DISTURBANCES (DC-CABLE FAULT)

For the testing of large disturbance at DC side, a 25Ω line-to-ground DC-cable fault is simulated at dc-side of VSC_3 at 0.3s lasting for 7 cycles (116 ms).

Fig. 11 shows the system dynamic response results of controlled DC branch current i_{12}, and bridge capacitor voltage u_c. The system recovers to its former state after the fault is cleared. The simulation results show that the system can endure DC side large disturbances.

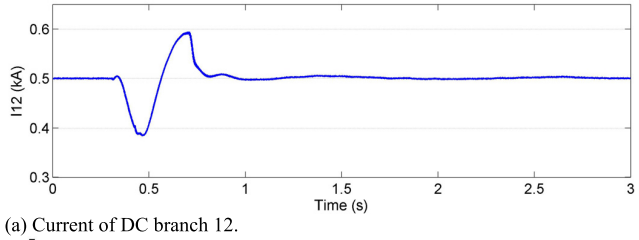

(a) Current of DC branch 12.

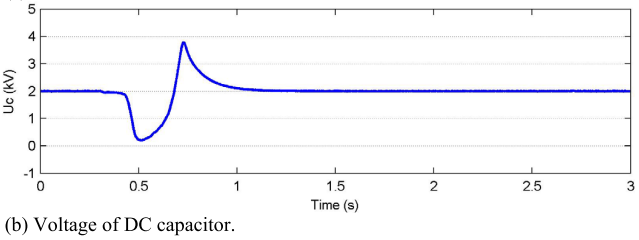

(b) Voltage of DC capacitor.

FIGURE 11. Dynamics of MTDC system against DC cable fault.

C. IMPACTS OF CONTROL PARAMETERS OF CFC ON VSC

The effects of the control parameters of CFC on VSC are studied in this section.

It has be found from modal analysis that different values of the CFC controller gains k_{pc1}, k_{ic1}, k_{pc2}, and k_{ic2} can affect dynamic stability of the integrated AC/DC system, especially on those VSC state variable related modes. The stable/unstable setting ranges of k_{pc1}, k_{ic1}, k_{pc2}, and k_{ic2} are obtained by the procedure shown in Fig. 12.

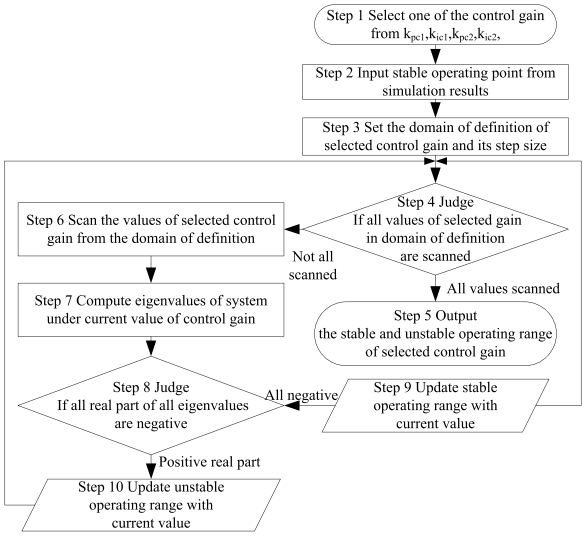

FIGURE 12. Flowchart to obtain stable operating range of CFC control gains.

For the given test system described in Section II, the stable/unstable setting ranges of k_{pc2} is listed as shown in Table 3, which is used as an example to investigate system dynamic stability when CFC controller gains are changed. Table 4 lists three different values of k_{pc2} ($k_{pc2} = 0.01, 0.1,$ and 1) and relevant modes. The corresponding values of $\lambda_{31,32}$ are $0.16 \pm j1.07$, $0.09 \pm j1.08$, and $-0.55 \pm j0.93$. It can be found that the system is stable only when $k_{pc2} \geq 1$.

TABLE 3. Setting ranges of k_{pc2}.

Value	Stability
$k_{pc2} \leq 0.231$	unstable, 1 positive pair of eigenvalues
$k_{pc2} \geq 0.231$	Stable

TABLE 4. Impact of k_{pc2} on the integrated MTDC/AC system dynamics.

Value	$\Lambda_{31,32}$	Stability
$k_{pc2} = 0.01$	$0.16 \pm j1.07$	unstable, 1 positive pair of eigenvalues
$k_{pc2} = 0.1$	$0.09 \pm j1.08$	unstable, 1 positive pair of eigenvalues
$k_{pc2} = 1$	$-0.55 \pm j0.93$	stable

The time-domain simulations in Fig. 13 are in line with the results shown in TABLE 4 when a small change of the reference is applied (i_{12ref} changes from 0.55 kA to 0.50 kA at 0.5s). Stable system dynamics can be achieved only when $k_{pc2} = 1$. Unstable oscillations are observed for $k_{pc2} = 0.1$

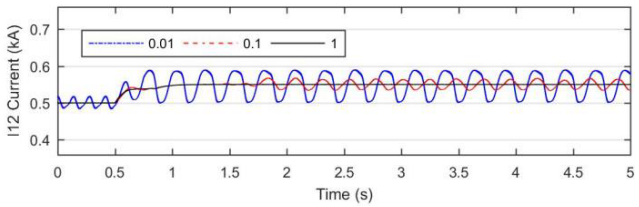

FIGURE 13. Dynamics of DC current i_{12} under different CFC control parameters.

and $k_{pc2} = 0.01$. It can also be seen that large k_{pc2} decreases the oscillation frequency and the settling time. The value of k_{pc2} has significant effects on state variables i_{12}, and y_2. These results demonstrate that the control parameters of CFC may cause instability of the system if they are not carefully-tuned.

As shown in Fig. 14, eigenvalue trajectories study is used to plot the movements of critical conjugate pairs so that the impacts of changing control parameters of CFC on VSC related modes can be analyzed. In Fig. 14, the control gain k_{pc2} varies from 0 (p.u.) to 1000 (p.u.) while the values of other control gains remain same. The purple arrows indicate the movements of conjugate pairs resulting from this variation of k_{pc2}. As shown in Fig. 14 (a), the imaginary parts of CFC related conjugate pairs (i_{12} and i_{13}) decrease as k_{pc2} increases, which indicates greater damping ratios of CFC related states. As shown in Fig. 14(a), two new VSC related conjugate pairs V_{dc2} and V_{dc1}(highlighted in blue) emerge as k_{pc2} increases. The movements of VSC related pairs (V_{dc2}, V_{dc1}, and VSCx_{32}) as shown in Fig. 14 (a)-(b) clearly present the impacts of CFC on VSC. The two conjugate pairs of V_{dc2} and V_{dc1} move towards left half of s-plane which indicates larger damping ratios of VSC related states V_{dc2} and V_{dc1}. The conjugate pairs of VSCx_{32} move towards right hand side indicating less damping ratios of VSCx_{32}. As shown in Fig. 14 (a)-(b), there are no significant movements of generator related poles, which indicates CFC has no significant impacts on synchronous machine related states.

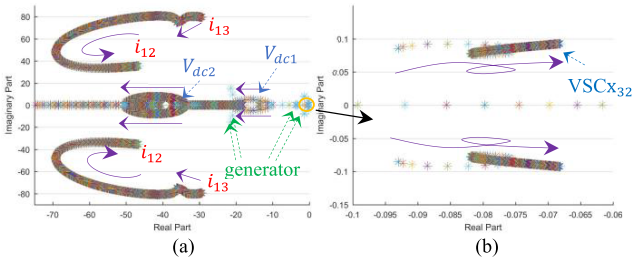

FIGURE 14. Eigenvalue trajectories of various CFC control parameter k_{pc2}.

Based on eigenvalue trajectory studies of CFC control gains, it can be summarized that the variation of CFC controller can affect dynamic stability of CFC and VSC related modes. These impacts of CFC on VSC can result in different damping characteristics of VSC related states, as CFC controller changes.

As listed in Table 5, three cases of different CFC control parameters are designed based on eigenvalue trajectories of various CFC control gains, to investigate their effects on the VSC controller related modes.

TABLE 5. Impacts of control parameters of CFC on VSC2 related modes.

	Related Eigenvalues	Stability
Case 1	$-0.13, -0.017 (\lambda_{39,43})$	Stable
Case 2	$-0.09 \pm j0.09 (\lambda_{39,40})$	Stable
Case 3	$0.02 \pm j0.10 (\lambda_{38,39})$	unstable, 1 positive pair of eigenvalues

Case 1: the control system of CFC is disabled as the base case to represent system without CFC control system.

Case 2: the gains of CFC control system are set the same as those in [25] ($k_{pc1} = 1, k_{ic1} = 1, k_{pc2} = 1, k_{ic2} = 1$), to represent the normal settings. The oscillations of VSC_2 controller related modes are seen from Table 5. The AC/DC system is stable for the first two cases.

Case 3: the gains of CFC control system are changed ($k_{pc1} = 0.01, k_{ic1} = 1000, k_{pc2} = 1, k_{ic2} = 1000$), to represent extreme or possible fault conditions of CFC control system. One conjugate pair of eigenvalues with positive real part is seen, which indicates small-signal instability.

Fig. 15 shows time-domain simulation results of three cases. As shown in Fig. 15, a small perturbation (DC branch current reference i_{12}^* changes from 0.55 kA to 0.5 kA) is applied to CFC at 0.15s. For Case 1, no significant change of VSC_2 auxiliary state variable x_3 is observed because the CFC control system is disabled. For Case 2, a small increase of x_3 at 0.2s can be seen. Then the value of x_3 recovers to its pre-disturbance level after a period time of oscillations. For Case 3, large unstable oscillations are seen.

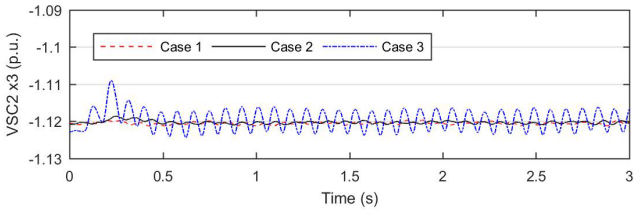

FIGURE 15. Effects of CFC control parameters on dynamics of VSC_2.

Simulation results are in line with the modal analysis results in Table 5, and illustrate that the CFC control system can affect dynamic performance of VSC converter controller. This effect can be severe and cause instability to the AC/DC system, for extreme DC CFC operating conditions.

The possible reason of these interactions between CFC control system and VSC controller can be the dynamical changing of the interfacing variables that relate CFC controlled variable and adjacent VSC controlled variable. For

instance, CFC controls DC branch current i_{12}, and VSC converter 2 controls DC voltage of VSC_2 V_{dc2}. And the relation between these two controlled state variables is given in equation 5a.

D. IMPACTS OF CONTROL PARAMETERS OF VSC ON CFC

The effects of the control parameters of VSC on CFC are studied in this section. Eigenvalue trajectory study is implemented to investigate potential impacts of different values of the control gains of VSC controller (k_{pdc}, k_{idc}, k_{pid}, k_{iid}, k_{pac}, k_{iac}, k_{piq} and k_{iiq}) on system dynamic stability of the integrated AC/DC system, especially on CFC state variable related critical modes. The stable setting ranges of the control parameters of VSC controller are obtained using the approaches presented in [9].

As eigenvalue trajectories shown in Fig. 16, the movements of critical conjugate pairs present the impacts of changing control parameters of VSC on CFC related modes. In Fig. 16, the control gain k_{idc} varies from 0 (p.u.) to 1000 (p.u.) while the values of other gains of VSC remain same. The purple arrows indicate the movements of conjugate pairs resulting from this variation of k_{idc}. As shown in Fig. 16(c), three new generator related conjugate pairs (highlighted in both green and purple arrow) emerge as k_{idc} increases. As shown in Fig. 16(b)-(d), the imaginary parts of generator related conjugate pairs increase as k_{idc} increases. This indicates greater damping ratios of corresponding generator related states. The movements of generator related pairs are less than those of CFC related and VSC related pairs as shown in Fig. 16(b) and (d). A new VSCx_{32} related conjugate pair emerges as k_{idc} increases as shown in Fig. 16(d). The VSC related conjugate pairs move towards left half of s-plane as k_{idc} increases, which indicates greater damping ratios of VSC related states. It should be noted that positive eigenvalues are seen in Fig. 16(d). This is due to the variation range of k_{idc} covers all stable and part of unstable operating range. As shown in Fig. 16(b) and (d), the movements of CFC related pairs (i_{12}, i_{13}, and CFCy_2) clearly present the impacts of VSC on CFC. The two conjugate pairs of i_{12} and i_{13} move towards right half of s-plane which indicates reduced damping ratios of CFC related states i_{12} and i_{13}. The conjugate pair of CFCy_2 moves towards left hand side indicating increased damping ratios of CFCy_2.

Based on eigenvalue trajectory studies of VSC control gains, it can be summarized that the variation of VSC controller can affect dynamic stability of synchronous generaors, VSC, and CFC related modes. These impacts of VSC on CFC can result in different damping characteristics of CFC related states, as VSC controller changes. And improper VSC controller tuning may cause instability to the integrated system.

As listed in Table 6, two cases with different VSC control parameters are designed based on eigenvalue trajectory studies of various VSC control gains, to investigate their effects on the CFC related system stability modes.

TABLE 6. Impacts of control parameters of VSC2 on CFC related modes.

	Related Eigenvalues	Stability
Case 4	$-0.09 \pm j0.09(\lambda_{39,40})$	stable
Case 5	$0.52 \pm j1.65(\lambda_{33,34})$	unstable, 1 positive pair of eigenvalues

Case 4: control parameters (value of the gains of proportional and integral controllers) of VSC_2 are set to normal operating values ($k_{pdc} = 7.52$, $k_{pac} = -10$, $k_{pid} = 0.3$, $k_{piq} = 0.3$, $k_{idc} = 1$, $k_{iac} = -1$, $k_{iid} = 1$, $k_{iiq} = 1$[9]). The system is stable.

Case 5: controller of VSC 2 is set with abnormal values ($k_{pdc} = 7.52$, $k_{pac} = -10$, $k_{pid} = 0.3$, $k_{piq} = 0.3$, $k_{idc} = 10$, $k_{iac} = -1000$, $k_{iid} = 1$, $k_{iiq} = 1$[9][9]) which represents extreme or faulty VSC operating condition. One conjugate pair of eigenvalues with positive real part can be seen which indicates small signal instability.

Fig. 17 shows time-domain simulation results for the effects of control parameters of VSC_2 on dynamic performance of CFC. As shown in Fig. 17, a small perturbation (DC branch current reference i_{12}^* changes from 0.5 kA to 0.55 kA) is applied to CFC at 0.3s. For Case 4, i_{12} quickly increases to 0.55 kA in response to the change of reference. For Case 5,

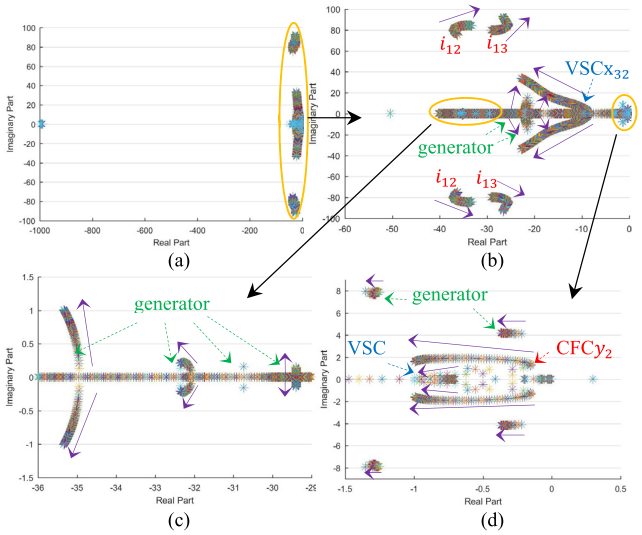

FIGURE 16. Eigenvalue trajectories of various VSC control parameter k_{idc}.

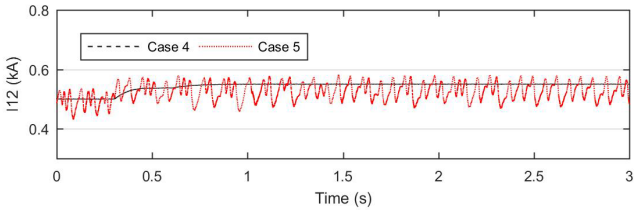

FIGURE 17. Effects of control parameters of VSC_2 on CFC.

large oscillations can be observed which indicates instability of CFC integrated DC network.

Simulation results demonstrate that the VSC controller can affect the dynamic performance of CFC. And this effect can be severe and cause instability of the CFC integrated DC network, for extreme VSC operating conditions.

IV. CONCLUSION

An integrated small-signal stability model for the study of interactions between CFC and VSC has been established. Modal analysis results have been verified by the dynamic simulations in RTDS under both small and large AC/DC disturbances (the AC system grounding fault applied in III.*B.2*) and DC system grounding fault applied in III.*B.3*)), which illustrates the incorporation of CFC has been shown to affect dynamic stability of the existing MTDC/AC system especially the adjacent VSC converters. The impacts of control parameters of CFC on the integrated AC/DC system with VSC and the impacts of VSC controller on the DC network with CFC have been investigated using both modal analysis and time-domain simulations. It has been found that the negative interactions between CFC and VSC could be severe and may cause instability to the integrated AC/DC system. The proposed modelling approach and methodology of analysis in this paper has provided a useful foundation that can be expanded for research of coordinated design of CFC control system and control system of VSC to avoid their possible negative interactions, as future work.

REFERENCES

[1] P. Bresesti, W. L. Kling, R. L. Hendriks, and R. Vailati, "HVDC connection of offshore wind farms to the transmission system," *IEEE Trans. Energy Convers.*, vol. 22, no. 1, pp. 37–43, Mar. 2007.

[2] L. Xu and L. Yao, "DC voltage control and power dispatch of a multi-terminal HVDC system for integrating large offshore wind farms," *IET Renew. Power Gener.*, vol. 5, no. 3, pp. 223–233, May 2011.

[3] L. Zhang, L. Harnefors, and H.-P. Nee, "Interconnection of two very weak AC systems by VSC-HVDC links using power-synchronization control," *IEEE Trans. Power Syst.*, vol. 26, no. 1, pp. 344–355, Feb. 2011.

[4] N. Flourentzou, V. G. Agelidis, and G. D. Demetriades, "VSC-based HVDC power transmission systems: An overview," *IEEE Trans. Power Electron.*, vol. 24, no. 3, pp. 592–602, Mar. 2009.

[5] X.-P. Zhang, "Multiterminal voltage-sourced converter-based HVDC models for power flow analysis," *IEEE Trans. Power Syst.*, vol. 19, no. 4, pp. 1877–1884, Nov. 2004.

[6] R. Preece and J. V. Milanovic, "Tuning of a damping controller for multiterminal VSC-HVDC grids using the probabilistic collocation Method," *IEEE Trans. Power Del.*, vol. 29, no. 1, pp. 318–326, Sep. 2014.

[7] S. Cole, J. Beerten, and R. Belmans, "Generalized dynamic VSC MTDC model for power system stability studies," *IEEE Trans. Power Syst.*, vol. 25, no. 3, pp. 1655–1662, Aug. 2010.

[8] N. R. Chaudhuri, R. Majumder, B. Chaudhuri, and J. Pan, "Stability analysis of VSC MTDC grids connected to multimachine AC systems," *IEEE Trans. Power Del.*, vol. 26, no. 4, pp. 2774–2784, Oct. 2011.

[9] G. O. Kalcon, G. P. Adam, O. Anaya-Lara, S. Lo, and K. Uhlen, "Small-signal stability analysis of multi-terminal VSC-based DC transmission systems," *IEEE Trans. Power Syst.*, vol. 27, no. 4, pp. 1818–1830, Nov. 2012.

[10] J. Beerten, S. Cole, and R. Belmans, "Modeling of multi-terminal VSC HVDC systems with distributed DC voltage control," *IEEE Trans. Power Syst.*, vol. 29, no. 1, pp. 34–42, Jan. 2014.

[11] R. Eriksson, "A new control structure for multiterminal DC grids to damp interarea oscillations," *IEEE Trans. Power Del.*, vol. 31, no. 3, pp. 990–998, Jun. 2016.

[12] N. R. Chaudhuri, R. Majumder, and B. Chaudhuri, "System frequency support through multi-terminal DC (MTDC) grids," *IEEE Trans. Power Syst.*, vol. 28, no. 1, pp. 347–356, Feb. 2013.

[13] N. R. Chaudhuri and B. Chaudhuri, "Adaptive droop control for effective power sharing in multi-terminal DC (MTDC) Grids," *IEEE Trans. Power Syst.*, vol. 28, no. 1, pp. 21–29, Feb. 2013.

[14] S. Liu, Z. Xu, W. Hua, G. Tang, and Y. Xue, "Electromechanical transient modeling of modular multilevel converter based multi-terminal HVDC systems," *IEEE Trans. Power Syst.*, vol. 29, no. 1, pp. 72–83, Jan. 2014.

[15] P. Kundur, *Power System Stability and Control*. New York, NY, USA: McGraw Hill, 1994.

[16] P. Kundur, "Definition and classification of power system stability IEEE/CIGRE joint task force on stability terms and definitions," *IEEE Trans. Power Syst.*, vol. 19, no. 3, pp. 1387–1401, May 2004.

[17] B. Pal and B. Chaudhuri, *Robust Control in Power Systems*. New York, NY, USA: Springer-Verlag, 2005.

[18] P. W. Sauer and M. A. Pai, *Power System Dynamics and Stability*. Englewood Cliffs, NJ, USA: Prentice-Hall, 1998.

[19] J. Arrillaga, *High Voltage Direct Current Transmission*. London, U.K.: Inst. Electr. Eng., 1998.

[20] J. Beerten, S. D'Arco, and J. A. Suul, "Identification and small-signal analysis of interaction modes in VSC MTDC systems," in *Proc. IEEE Power Energy Soc. General Meeting (PESGM)*, Boston, MA, USA, Jul. 2016, p. 1.

[21] C. D. Barker and R. S. Whitehouse, "A current flow controller for use in HVDC grids," in *Proc. 10th IET Int. Conf. AC DC Power Trans. (ACDC)*, Birmingham, U.K., Dec. 2012, pp. 1–5.

[22] D. Jovcic and B. T. Ooi, "Developing DC transmission networks using DC transformers," *IEEE Trans. Power Del.*, vol. 25, no. 4, pp. 2535–2543, Oct. 2010.

[23] W. Chen, X. Zhu, L. Yao, X. Ruan, Z. Wang, and Y. Cao, "An interline DC power-flow controller (IDCPFC) for multiterminal HVDC system," *IEEE Trans. Power Del.*, vol. 30, no. 4, pp. 2027–2036, Aug. 2015.

[24] N. Deng, P. Wang, X.-P. Zhang, G. Tang, and J. Cao, "A DC current flow controller for meshed modular multilevel converter multiterminal HVDC grids," *CSEE J. Power Energy Syst.*, vol. 1, no. 1, pp. 43–51, Mar. 2015.

[25] N. Deng, P. Wang, and X.-P. Zhang, "Small-signal stability analysis and control system design of a meshed multi-terminal high-voltage direct current grid with a current flow controller," *Electr. Power Compon. Syst.*, vol. 44, no. 10, pp. 1126–1137, 2016.

[26] P. Wang, N. Deng, X.-P. Zhang, and N. Jiang, "Parametric analysis and optimization of a DC current flow controller in meshed MTDC grids," *IEEE Access*, vol. 7, pp. 87960–87976, 2019. [Online]. Available: https://ieeexplore.ieee.org/document/8747439

[27] S. Balasubramaniam, C. E. Ugalde-Loo, and J. Liang, "Series current flow controllers for DC grids," *IEEE Access*, vol. 7, pp. 14779–14790, 2019.

[28] S. Balasubramaniam, C. E. Ugalde-Loo, J. Liang, and T. Joseph, "Power flow management in MTdc grids using series current flow controllers," *IEEE Trans. Ind. Electron.*, vol. 66, no. 11, pp. 8485–8497, Nov. 2019.

[29] J. Sau-Bassols, E. Prieto-Araujo, O. Gomis-Bellmunt, and F. Hassan, "Series interline DC/DC Current Flow Controller for meshed HVDC grids," *IEEE Trans. Power Del.*, vol. 33, no. 2, pp. 881–891, Apr. 2018.

[30] J. Sau-Bassols, E. Prieto-Araujo, O. Gomis-Bellmunt, and F. Hassan, "Selective operation of distributed current flow controller devices for meshed HVDC grids," *IEEE Trans. Power Del.*, vol. 34, no. 1, pp. 107–118, Feb. 2019.

[31] P. Wang, N. Deng, and X.-P. Zhang, "Droop control for a multi-line current flow controller in meshed multi-terminal HVDC grid under large DC disturbances," *IEEE Power Energy Technol. Syst. J.*, vol. 5, no. 2, pp. 35–46, Jun. 2018.

[32] S. Balasubramaniam, C. E. Ugalde-Loo, J. Liang, T. Joseph, R. King, and A. Adamczyk, "Experimental validation of dual H-bridge current flow controllers for meshed HVdc grids," *IEEE Trans. Power Del.*, vol. 33, no. 1, pp. 381–392, Feb. 2018.

RUI GUAN received the B.Eng. degree (Hons.) and the Ph.D. degree in electrical engineering from the University of Birmingham in 2014 and 2018, respectively. He is currently with Global Energy Interconnection Development and Cooperation Organization (GEIDCO). His main research interests include HVDC system and FACTS.

NA DENG received the B.Eng. degree from the Huazhong University of Science and Technology (HUST), China, in 2011, and the Ph.D. degree from the University of Birmingham, Birmingham, U.K., in 2015. She is currently with the Jiangsu Industrial Technology Research Institute (JITRI). Her research interest includes the applications of dc/dc and ac/dc converters in HVDC systems and microgrids.

YING XUE received the B.Eng. degree in electrical engineering from the Huazhong University of Science and Technology (HUST), Wuhan, China, and the University of Birmingham, Birmingham, U.K., in 2012, and the Ph.D. degree in electrical engineering from the University of Birmingham in 2016. He is currently a Lecturer with the University of Birmingham. His main research interest includes HVDC modeling and control.

XIAO-PING ZHANG (M'95–SM'06) is currently a Professor of electrical power systems with the University of Birmingham, U.K., and he is also the Director of the Smart Grid, Birmingham Energy Institute and the Co-Director of the Birmingham Energy Storage Center. He has coauthored the first and second edition of the monograph *Flexible AC Transmission Systems: Modeling and Control*, (Springer, 2006 and 2012). He has coauthored the book *Restructured Electric Power Systems: Analysis of Electricity Markets With Equilibrium Models*, (IEEE Press/Wiley, 2010).